Lysophospholipid headgroup size, and acyl chain length and saturation differentially affect vacuole acidification, Ca^{2+} transport, and fusion

Chi Zhang [1,3], Yilin Feng [1,3], Jorge D. Calderin [1], Adam Balutowski [1], Razeen Ahmed [1], Charlie Knapp [1] and Rutilio A. Fratti [1,2,*]

1. Dept. of Biochemistry, University of Illinois Urbana-Champaign, Urbana, IL, 61801
2. Center for Biophysics & Quant, Biol., Univ. of Illinois Urbana-Champaign, Urbana, IL, 61801
3. These authors contributed equally

* Address correspondence to: Rutilio A. Fratti (rfratti@illinois.edu)

Running title: Lysophospholipids affect ion transport and fusion

Keywords: Acidification, Calcium, fusion, Lysophosphatidylcholine, Lysophosphatidic acid. SNARE, V-ATPase

ORCID ID: *Rutilio Fratti* - 0000-0001-9109-6666

ABSTRACT

SNARE-mediated membrane fusion is regulated by the lipid composition of the engaged bilayers. Lipid composition impacts fusion through direct protein lipid interactions or through modulating the physical properties of membranes at the site of contact, including the induction of positive curvature by lysophospholipids (LPLs). The degree of positive curvature induced is due to the length and saturation of the single acyl chain in addition to the size of the head group. Here we examined how yeast vacuole fusion and ion transport were differentially affected by changes in lysolipid properties. We found that lysophosphatidylcholine (LPC) with acyl chains containing 14-18 carbons all inhibited fusion with IC_{50} values ranging from ~40-120 μM. The monounsaturation of LPC-18:1 had no effect when compared to its saturated counterpart LPC-18:0. On the other hand, head group size played a more significant role in blocking fusion as lysophosphatidic acid (LPA)-18:1 failed to fully inhibit fusion. We also show that both Ca^{2+} uptake and SNARE-dependent Ca^{2+} efflux was sensitive to changes in the acyl chain length and saturation of LPCs, while LPA only affected Ca^{2+} efflux. Finally, we tested these LPLs on vacuole acidification by the V-ATPase. This showed that LPC-18:0 could fully inhibit acidification whereas other LPCs had moderate effects. Again, LPA had no effect. Together these data suggest that the effects of LPLs were due to a combination of head group size and acyl chain length leading to a range in degree of positive curvature.

INTRODUCTION

Eukaryotes use SNARE-mediated membrane fusion to transport cargo between organelles as well as secretion or endocytosis at the plasma membrane. Although the final stage of fusion is driven by SNAREs, the full pathway is composed of multiple phases, each controlled by a distinct set of proteins and lipids. In general, membrane lipids can regulate protein function through two mechanisms. One mechanism is through the specific interactions of lipids and proteins. This is exemplified by the direct interactions of phosphoinositides and lipid-binding protein domains including PH, PX and FYVE domains (1–3).

Another mechanism of lipid-induced protein control occurs through the indirect effects of the physical aspects of membranes itself such as curvature, fluidity and thickness (4–6). These properties are regulated by levels of specific lipids such as cholesterol, sphingolipids, and non-specifically by acyl chain saturation and length. Membrane curvature and fluidity can also be

affected by lysophospholipids (LPL) and free fatty acids (FFA). LPLs are generated through the action of phospholipase A1 (PLA1) or PLA2 on a glycerophospholipid such as phosphatidylcholine (PC) that releases the fatty acid from the sn-1 or sn-2 position, respectively and generating a lysolipid containing a single acyl chain. Lysolipids affect the membrane by inducing positive curvature. LPL induced membrane curvature is due to their inverted cone shape with a large headgroup and narrow tail. The degree of curvature depends on acyl chain length and saturation in addition to the headgroup size (7, 8). The smallest head group is a single phosphate on lysophosphatidic acid (LPA). Larger headgroups range from ethanolamine (LPE, lysophosphatidylethanolamine), serine (LPS, lysophosphatidylserine), choline (LPC, lysophosphatidylcholine) and inositol (LPI, lysophosphatidylinositol). The acyl chains of lysolipids can range from 10 to 20 carbons that are saturated or contain one or more double bonds.

Most LPLs are resistant to bilayer translocation, i.e. Flip-Flopping, thus preventing equilibration between leaflets after PLA activity. LPLs with 12 carbon chains or shorter can flip-flop across membrane leaflets (Seeman 72; Lieber 84). Longer LPLs that do not flip lead to a pronounced increase in positive curvature of the leaflet exposed to PLA. In erythrocytes, LPC can be generated on either side of the plasma membrane causing distinct morphological features (9). LPC generation on the outer leaflet of erythrocytes produces pointed protrusions to form echinocytes, whereas production on the inner leaflet is stomatocytogenic in that it causes the formation of pits or invaginations on the cell surface. In both cases, the deformation is caused by positive curvature induced by local LPC production (9). The severity of positive curvature, due to increased headgroup size, can influence membrane thinning as shown by the dimerization of gramicidin channels that can vary by >100 fold when comparing LPC and LPI. (10).

In addition to membrane deformation, LPL can affect ion channels, which plays a critical role in vacuole homeostasis. In particular, LPL differentially regulates Ca^{2+}/Mg^{2+} ATPase function in a manner dependent on acyl chain length and saturation and headgroup (Tokumura *et al*, 1985). The transient receptor potential (TRP) Ca^{2+} channel TRPC5 is activated by LPC and LPI with acyl chains of 14 carbons (C14) or bigger, whereas C12 LPL had no effect (13). Importantly, LPL can affect Ca^{2+} transport in a protein free manner through the formation of transient Ca^{2+} pores as seen in lymphoma cells (12). Altering membrane curvature not only alters ion transport but can affect membrane fusion. Largely, this occurs through effects on the formation and stability of hemifusion diaphragms and the transition to full bilayer fusion (14). LPC can also affect fusion at the priming stage when inactive SNARE complexes are disrupted by NSF (15).

LPLs can directly affect membrane fusion, whether it be the fusion of liposomes with cells (16), microsome fusion (17) or viral fusion (18, 19). The effect of LPLs has been targeted to the transition between hemifusion and full bilayer mixing. How this occurs has been attributed to various mechanisms including the induction of positive curvature LPC.

Yeast vacuole fusion serves as a model in vitro system to examine the role of specific proteins and lipids throughout the fusion pathway. Previous studies have focused on glycerophospholipids and sphingolipids on the different stages of fusion. SNARE priming by Sec18/NSF is regulated by the conversion of phosphatidic acid (PA) to diacylglycerol (DAG) by the PA phosphatase Pah1, as well as the presence of ergosterol and PI(4,5)P_2 (phosphatidylinositol 4,5-bisphosphate) (20–23). Vacuole tethering is controlled by the Rab GTPase Ypt7 and its effector complex HOPS, which in turn is controlled by the presence of various phosphoinositides (PI) and sphingolipids (24–27). Tethering leads to docking and SNARE pairing that occurs at distinct membrane contact points termed vertex domains which forms interdependently with PI3P, PI(4,5)P_2, DAG and ergosterol . The formation of SNARE complexes between membranes leads to the release of Ca^{2+} stores from the vacuole lumen that is controlled in part by PI(3,5)P_2 (28, 29).

Prior to full content mixing, the outer leaflets of the vacuoles undergo hemifusion that is controlled in part by PI(3,5)P_2 (30). Between hemifusion and full fusion others have shown that the integral membrane subunit complex of the V-ATPase (Vo) can form complexes in trans between membranes (31). This penultimate step can be blocked by the addition LPC with 10-14 carbon acyl chains, with increased efficiency due to longer acyl chains (32). This is similar to findings from Chernomordik et al. where LPC with acyl chains ranging from 12-18 carbons inhibited the fusion of erythrocytes to fibroblasts (18).

In this study we examine LPC with acyl chains containing 14-18 carbons on vacuole fusion, Ca^{2+} transport and V-ATPase mediated acidification of the vacuole lumen. In addition, we compare the role of headgroup size by comparing of LPA and LPC with identical monounsaturated 18:1 carbon acyl chains. We found that each of the LPL inhibited fusion and vacuole acidification with varying efficiency dependent mostly on head group size, whereas Ca^{2+} transport was mostly affected by acyl chain length.

RESULTS

LPC and LPA inhibit vacuole fusion

Previous studies have shown that vacuole fusion can be inhibited by LPC with acyl chains as long as 14 carbons with an IC_{50} ranging from 30 μM for LPC-14 to ~700 μM for LPC-10 (32). Chernomordik et al. found that LPC-14 inhibited cell-cell fusion with and IC_{50} ~20 μM and ~0.7 μM for LPC-16/18. Together these studies showed that the ability to inhibit fusion was proportional to the LPC tail length. Here we bridge the two approaches with isolated yeast vacuoles and a range of LPLs from LPC-14 to LPC-18 and include the unsaturated LPC-18:1 and LPA-18:1 to compare head group size. Vacuole fusion is determined by an endpoint colorimetric content mixing assay. The fusion reactions contain a 1:1 mixture of vacuoles of an enzyme and substrate. The substrate vacuoles harbor the inactive alkaline phosphatase zymogen pro-Pho8 and lack the processing protease Pep4 (*pep4*Δ *PHO8*) (33). The enzyme vacuoles harbor Pep4 but lack pro-Pho8 (*PEP4 pho8*Δ) (34). When vacuole contents mix the Pep4 protease gains access to the pro-Pho8 substrate and cleaves the autoinhibitory end of the zymogen to produce active Pho8. At the end of the reactions the membranes are dissolved with a detergent and Pho8 activity is measured with the colorimetric conversion of colorless PNPP to yellow PNP that can be measured at 400 nm visible light absorbance. Fusion data was pooled from 3 or more separate trials and normalized to the untreated control set to 1. Thus, we present the data are relative values. The baseline fusion (negative control) was determined by setting an untreated fusion reaction on ice for the duration of the experiment. The ice condition ranges from 10-20% of the maximum.

In these experiments we added dose curves of each lysolipid at the start of the reaction and incubated in a circulating water bath for 90 min at 27ºC. We found that vacuole fusion was inhibited by LPC-14 with an IC_{50} of 118 μM, which was greater that the 30 μM IC_{50} that was previously reported **(Fig. 1A)** (32). The difference could be due changes in incubation time where they incubated for 60 min while we used 90 min incubation times. Furthermore, LPC-14 did not fully inhibit at concentrations as high as 500 μM. When testing LPC-16 and LPC-18 we found that they followed the trend of increased inhibition linked to tail length. Both LPC-16 and -18 had IC_{50} values of 44 μM and the fully inhibited down to the ice control **(Fig. 1B and C, respectively)**. This was also higher than the Chernomordik study, however, their assay was clearly different in that it used whole cells and plasma membrane fusion. In addition, they used R18 dye dequenching which also measures outer leaflet fusion (i.e., hemifusion) and not necessarily full content mixing. Nevertheless, the increase in fusion inhibition mapped with the increase in acyl chain length.

We next asked if acyl chain saturation played a significant role in blocking fusion. To address this, we used LPC-18:1 with a double bond in *cis* at carbon 9 (*cis*-Δ^9), i.e., oleic acid. Surprisingly, the unsaturation had no further effect on fusion. LPC-18:1 inhibited vacuole fusion with an IC_{50} of 37 μM **(Fig. 1D, blue)**. That said, the LPC18:1 maximum inhibition at 500 μM was above the ice control (>20% of maximum), whereas LPC-18:0 inhibited down to 10% of maximum matching the ice control, suggesting that the increase in tail width of provided by the unsaturation could impact how well LPC induces positive curvature to affect fusion. Finally, we examined the role of headgroup size by comparing LPC-18:1 with LPA-18:1. This showed that LPA poorly affected vacuole fusion with an IC_{50} of 243 μM, which is an underestimate since maximum inhibition only reached 40% of maximum at 500 μM **(Fig. 1D, green)**. This suggests that head group affected the inhibitory effect lysolipids more than acyl chain length.

Ca^{2+} transport across the vacuole membrane is sensitive to lysolipids

Vacuoles are the main storage unit of Ca^{2+} in yeast instead of the endoplasmic reticulum. Vacuoles contain mM levels of Ca^{2+} that is mostly complexed to polyphosphate, leaving μM free Ca^{2+} (35). The yeast vacuole contains the high affinity Ca-ATPase pump Pmc1 and the low affinity Ca^{2+}/H^+ exchanger Vcx1 (36, 37). Vacuoles also contain the TRP homolog Yvc1 which releases Ca^{2+} upon osmotic stress induced vacuole fission which is regulated by the production of $PI(3,5)P_2$ by the PI3P kinase Fab1 (38–41).

During vacuole fusion SNAREs from separate vesicles join into a parallel coiled-coil containing four SNARE motifs. This leads to the release of Ca^{2+} from the vacuole lumen through a mechanism that is independent of the TRP channel Yvc1, yet remains sensitive to levels of $PI(3,5)P_2$ (28, 29). Since SNARE-dependent Ca^{2+} release during fusion is likely mechanosensitive we next tested the effects of lysolipids. Using a real-time fluorescence assay we can measure the kinetics of Ca^{2+} uptake and efflux in the same experiments (42, 43). Extraluminal Ca^{2+} is detected by a probe that only fluoresces when bound to Ca^{2+}. We use Cal520 conjugated to dextran to measure Ca^{2+} transport. There is sufficient extraluminal Ca^{2+} (~0.5-1 μM) in reaction system that fluorescence starts high and rapidly decreases upon the addition of ATP, which activated Pmc1 and the uptake of Ca^{2+} into the vacuole lumen and is monitored by the loss of Cal520 fluorescence. Once SNAREs form complexes in trans Ca^{2+} is released back into the extraluminal space and Cal520 increases in fluorescence. As a control for SNARE-dependent Ca^{2+} efflux we include anti-Sec17 IgG as a control that prevents SNARE activation (44). This is characterized by the uptake of Ca^{2+} without the subsequent release.

Here, we tested the effects of adding lysolipids on Ca^{2+} uptake and efflux. First, we added lysolipids at the start of the reactions, 30 sec before adding ATP. Starting with LPC-14, we observed an inhibition of Ca^{2+} uptake as shown by the partial loss of fluorescence that stopped at 10 min and leveled off, thus masking any effect on efflux **(Fig. 2A-C)**. Based on the fusion data in Figure 1, we imagined that LPC-16 would have a stronger effect on Ca^{2+} uptake versus LPC-14. Unexpectedly, we observed no effect on Ca^{2+} uptake as show by the loss of fluorescence identical to the untreated control **(Fig. 2D-E)**. While uptake was not affected, we did observe a complete loss of Ca^{2+} efflux with 125 μM and 250 μM LPC-16 and a partial block with as little as 50 μM, which is near the IC_{50} for blocking fusion **(Fig. 2D and F)**. Finally, we examined how extending LPC to containing a saturated 18 carbon acyl chain. We found that adding LPC-18:0 at the start of the Ca^{2+} assay had an effect that was a mix of LPC-14 and LPC-16. The uptake of Ca^{2+} was inhibited by 250 μM LPC-18:0, while 125 μM kept uptake from reaching the anti-Sec17 plateau suggesting that uptake was partially blocked **(Fig. 2G & H)**. The lowest concentration tested (50 μM LPC-18:0) had no effect on uptake, however, it had a significant effect on release at 30 min **(Fig. 2G & I)**.

Next, we tested whether acyl chain desaturation and lysolipid head group size affected Ca2+ transport. First, we tested LPC-18:1 *cis*-Δ^9 and found that it inhibited uptake at 250 μM at 10 min similar to what we saw with the saturated version of the lipid **(Fig. 2J & K)**. At lower concentrations we observed that it significantly blocked Ca^{2+} efflux **(Fig. 2J & L)**. This was again similar to what occurred with saturated LPC-18:0. Together this suggests that a single unsaturation does not affect LPC with 18 carbon acyl chains. This does not exclude the possibility that higher levels of unsaturation would not have an effect. Finally, we asked if the headgroup size of the lysolipid would have an impact on vacuolar Ca^{2+} transport. To answer this, we used the smallest of the headgroups which is the single phosphate at position sn-3 of LPA. Unexpectedly, we found that LPA-18:1 had no effect on Ca^{2+} uptake or efflux when added at the beginning of the experiment **(Fig. 2M-N)**. Thus, we conclude that the size of the head group plays a critical role in altering Ca^{2+} flux during fusion. This was likely due to changes in the degree of curvature caused by a phosphocholine versus a single phosphate.

In previous studies we have found that the effect of agents on Ca^{2+} transport can vary depending on the time of addition. In Figure 2 we added each of the lysolipids at the start of the assay and monitored both uptake at 10 min and efflux at 30 min. Some of the lysolipids blocked uptake, thus

masking any effect on the subsequent efflux that occurs during the docking stage of the pathway. We next tested if the lysolipids could alter efflux alone when added at 10 min when uptake has plateaued. Starting with the shortest LPC, we tested the 14 carbon myristyl form. Adding LPC-14 at first caused a blip of Ca^{2+} detection that was quickly reabsorbed. This was likely due to trace amounts of Ca^{2+} in the dissolved LPC. That said, we observed delayed Ca^{2+} efflux for nearly 10 min after which the reactions rapidly recovered to mirror the untreated control at 30 min **(Fig. 3A-B)**. This occurred independent of the concentration range tested. Adding LPC-16 at 10 min also caused a blip in signal followed by a rapid reuptake of Ca^{2+} **(Fig. 3C-D)**. However, unlike LPC-14, adding the palmitoyl form blocked Ca^{2+} efflux with equal intensities at the three concentrations tested. This suggests that LPC-16 could have an at concentrations below 50 μM. Interestingly, stearoyl LPC-18:0 had no striking effect on efflux even though the effect of 50 μM was statistically significant **(Fig. 3E-F)**. Together this indicates that the most effective acyl chain length for altering Ca^{2+} efflux was 16 carbons. Since IC_{50} values for inhibiting fusion were identical for LPC-16 and -18, the difference in altering Ca^{2+} transport suggest that there is at least one additional effect triggered by LPC-18 to alter overall fusion.

When added at the start of the reaction the unsaturated oleoyl LPC-18:1 had the same effect at the unsaturated stearoyl form. When added after Ca^{2+} uptake we found that 250 μM had a rapid rise in efflux beyond what could be attributed to trace levels **(Fig. 3 G-H)**. After the rapid rise, the rate leveled off to match the untreated control. Surprisingly, lower levels of LPC-18:1 potently inhibited Ca^{2+} efflux. While this may appear contradictory, this could be attributed to differential effects on uptake and efflux which have previously detected with altering $PI(3,5)P_2$ (29). Briefly, our previous work suggested that uptake by the high affinity pump Pmc1 is constant throughout the reaction and that efflux appears when a separate mechanism masks further Pmc1 activity. Pmc1 activity can also be augmented to mask Ca^{2+} efflux.

Another difference appeared when we tested the late addition of LPA-18:1 to the Ca^{2+} transport assay. When added at the start LPA had no effect on uptake or efflux; however, when added after uptake was complete, we observed a dose dependent inhibition of Ca^{2+} efflux **(Fig. 3 I-J)**. This difference could be due to the extraluminal Ca^{2+} concentration at the time of addition. For instance LPA forms type-1 lipid micelles in the absence of divalent cations while in its presence LPA is driven to form a complexes with the cation in a bilayer (45). Differences could also be due to changes in charge. When free, the LPA phosphate has a -2 charge while it has a -1 change in

acidic environments. Hydrogen bonding with PE can also increase the negative charge of the LPA phosphate ester.

Vacuole acidification is inhibited by LPC

Yeast vacuoles are acidic lysosomal compartments that aid in the degradation of macromolecules into their constituent building blocks. This requires an acidic environment that activates digestive enzymes at the site of activity and not during their trafficking through the endoplasmic reticulum, Golgi and transport vesicles. Vacuole acidification is carried out by the vacuolar ATPase (V-ATPase) that is composed of two complexes. The V_O complex is embedded in the vacuole membrane and contains the hemi-channel that transports H^+ from the cytoplasm into the vacuole lumen. The transport up the chemical gradient requires energy that is generated through ATP hydrolysis by the cytoplasmic V_1 complex. The V_1-V_O holoenzyme is stabilized in part through the interactions between the V_O subunit Vph_1 and the regulatory lipid $PI(3,5)P_2$ (46, 47). This lipid also regulates vacuole fusion at the hemifusion stage (29, 30). V-ATPase activity is attenuated by the lack of sphingolipids containing very long chain fatty acids which increases fluidity and inhibits vacuole fusion (27). The activity of V-ATPase activity is also sensitive to fluidity as the fluidizing anesthetic dibucaine can potently inhibit vacuole acidification. Aside from fluidity, we have found that V-ATPase activity is sensitive to high Ca^{2+}, which inhibits fusion and can affect how LPA interacts with membranes (48). Finally, H^+ can be rapidly expelled from the vacuole in the presence of the lanthanides La^{3+} and Gd^{3+} that can block Ca^{2+} transport and mimics the effect of deleting both *PMC1* and *VCX1* (29, 49). Based on this and our data showing that lysolipids can affect Ca^{2+} transport, we next asked if they can affect vacuole acidification.

To measure vacuole acidification, we used a fluorescence shift assay and acridine orange (AO). At near-neutral pH AO fluoresces at 520 nm when excited at 488 nm (50). AO is transported into acidic compartments where it is protonated and becomes dimeric, which in turn traps the dye in the acidic lumen and alters its fluorescence. AO in acidic environments emits at 680 nm as fluorescence at 520 nm is diminished as a metachromatic shift (49, 51, 52). This allows for real-time tracking of vesicle acidification.

To examine the effects of lysolipids on V-ATPase activity we first tested LPC-14. Reactions were with buffer alone or increasing concentrations of LPC-14 for 30 sec after which ATP was added to start V-ATPase activity. A separate reaction lacked ATP to serve as a negative control. Reactions were run for 600 sec at which point 30 μM FCCP was added to each well to equilibrate

H^+ concentrations across the membrane and retore AO fluorescence to 520 nm. This showed that the decrease in fluorescence was indeed due to vesicle acidification and not bleaching or denaturing of the dye.

Figure 4A shows the acidification of vacuoles relative to the decrease in AO fluorescence at 520 nm. The black trace shows the positive control with ATP and no LPC. The decrease in fluorescence plateaus at ~400 sec after the addition of ATP. In the absence of ATP, AO fluorescence is maintained throughout the incubation (dotted trace). The addition of LPC-14 decreased the rate of acidification in a dose dependent manner. That said, each concentration of LPC-14 caught up with the untreated control by 600 sec. When we measured fluorescence at 400 sec for multiple experiments, we found that LPC-14 significantly attenuated H^+ transport (**Fig. 4 B)**. This proportionally matched its effect on Ca^{2+} uptake when added at T=0.

We next tested the effects of longer saturated acyl chains on V-ATPase activity. Like LPC-14, the addition of LPC-16 at the start slowed V-ATPase activity in a dose dependent manner **(Fig. 4 C-D)**. In addition, the LPC-16 treated samples caught up with the control by 600 sec. Interestingly, treating reactions with LPC-18:0 appeared to fully inhibit V-ATPase activity as the treated samples never caught up with the control **(Fig. 4 E-F)**. Together these data indicate that the V-ATPase is sensitive to acyl chain length, likely corresponding to changes in membrane fluidity and curvature. To further test this notion, we used oleoyl LPC-18:1. Oleic acid is known to increase fluidity whereas the saturated 18 carbon fatty acid decreases fluidity. We found that LPC-18:1 only slowed V-ATPase activity, and the treated samples caught up with the control as seen with the with the shorter acyl chain containing LPCs **(Fig. 4 G-H)**. This is in keeping with the idea that fluidity impacts V-ATPase activity. Finally, we asked if an oleoyl lysolipid with a small head group would have the same effect as LPC-18:1. For this we used LPA-18:1 and observed that vacuole acidification was unaffected **(Fig. 4 I-J)**. This was similar to the lack of an effect of LPA-18:1 on Ca^{2+} uptake and goes with the link between Ca^{2+} gradients and V-ATPase function. This also shows that an oleoyl acyl chain alone is not sufficient in altering vacuole acidification. Instead, it appears that inhibiting V-ATPase function with lysolipids is linked to the length of a saturated acyl chain as well as the degree of membrane curvature affected by the lysolipid head group.

While LPA had no effect on Ca^{2+} or H^+ transport when added LPA at the beginning of the experiments, we did find that it altered Ca^{2+} efflux when added after 10 min of incubation. As such, we examined the effect of adding lysolipids after vacuole acidification had reached a plateau. We

found that LPC-14 had no significant effect on maintaining acidification levels **(Fig. 5 A-B)**. In contrast, LPC-16 **(Fig. 5 C-D)**, LPC-18:0 **(Fig. 5 E-F)** and LPC-18:1 **(Fig. 5 G-H)** all reversed V-ATPase activity as shown by the rapid rise in AO fluorescence, albeit to different degrees. This suggested that once acidified, maintaining the H^+ gradient was sensitive to acyl chains of 16 or more carbons in length and independent of hydrocarbon mono-unsaturation. Importantly, LPA-18:1 had no effect when added late similar to its early addition. This suggested that head group size, and thus degree of positive curvature was critical in the inhibition of vacuole acidification.

DISCUSSION

Vesicle fusion is triggered by the pairing of SNARE complexes and the transfer of force to their respective membranes. That said, the ability of SNAREs to carry this out is dependent on a suite of physical and chemical requirements, including the formation and maintenance of electrochemical gradients, ion gradients and membrane potential. Additional layers of control involve signal transduction and spatiotemporal modifications of signaling lipids phosphoinositides, PA and DAG. Lipids are modified by kinases, phosphatases and lipases that produce free fatty acids and lysolipids.

In this study we examined the role of LPLs on vacuole fusion, Ca^{2+} transport and V-ATPase activity. Specifically, we tested the roles of acyl chain length and saturation as well as headgroup size. In general, we found that the LPL traits tested had differential effects on fusion and ion transport. Each of the lipids inhibited vacuole fusion with varying efficacy. For fusion the critical factor was headgroup size with LPA being the least effective relative to the LPC variants tested. Thus, acyl chain length and monounsaturation is of little importance for overall fusion inhibition. Headgroup size on the other hand had a large effect on fusion, suggesting that the degree of positive curvature is proportional to how well and LPL inhibits fusion. To illustrate, the larger choline headgroup of oleoyl LPC leads has an intrinsic positive curvature of +38 Å versus the single phosphate on oleoyl LPA with an intrinsic curvature of +20 Å (8, 53). In addition to changes in curvature, it is possible that the negative charge of LPA influences how well fusion is blocked. For instance, the negative charge of LPA can interact with Ca^{2+} to reduce its effect on curvature by inducing bilayer formation (45).

While LPC variants with 14-18 carbons made little difference in how well LPCs inhibits fusion other a study by Reese and Mayer looked at shorter acyl chains variants and found that inhibition

was relative to hydrocarbon length. Specifically, they found that LPC-14, -12, -10 and -8 inhibited vacuole fusion with IC_{50} values of ~30 μM, ~100 μM, ~400 μM, and 3 mM, respectively (32). Together with our data, we can conclude that acyl chain length is important until efficacy plateaus at 14 carbons. Their study went on to show that the block in fusion was between SNARE pairing and hemifusion. A critical step between these phases is the release of luminal Ca^{2+} upon trans-SNARE complex formation (28). The effects of lysolipids on Ca^{2+} transport has been shown with multiple transporters in different cell types, however, these studies mostly focused on the plasma membrane and cytosolic Ca^{2+} and did not consider effects on lysosomal transport.

Among the types of Ca^{2+} transporters affected by lysolipids are L-type voltage dependent channels. In myocytes production of LPC stimulates L-type channels leading to Ca^{2+} overloading that was inhibited by the L-type inhibitor nimodipine (54). The same is seen in Drosophila S2 cells (55). This effect was only seen with stearoyl LPC-18:0 and palmitoyl LPC 16:0 worked, whereas LPC-18:1, -18:2, -18:3 had no effect. Furthermore, LPE, LPA, LPI and LPS did not trigger Ca^{2+} accumulation. Transport through L/P-type channels including the yeast Ca^{2+} P-type ATPase are sensitive to channel blockers such as verapamil.

Lysolipids can also affect Ca^{2+} through mechanosensitive channels including members of the TRP family. For example, TRPC5 is activated by LPC and LPI with acyl chains containing 14 or more carbons (13). That said the same study showed that lysolipids had no effect on TRPC2. LPC and LPI also induce Ca^{2+} influx via TRPv2 when the acyl chains were at least 16 carbons in length. This led to an increase cell migration in prostate cancer cells, suggesting that actin dynamics were also affected (56). In this case, headgroup size was also considered and revealed that the smaller headgroups LPA and LPE had no effect. The effect of headgroup size is not consistent as shown in lens cells where LPA triggers Ca^{2+} flux through a mechanosensitive channel, while LPC had no effect (57). In these cases, lysolipid triggered transport through mechanosensitive ion channels are not affected by inhibitors such as verapamil and nicardipine, thapsigargin or blocking phospholipase C with U73122. Instead, mechanosensitive channels are inhibited by lanthanides.

So, how do lysolipids affect yeast vacuole Ca^{2+} transport? Vacuoles move Ca^{2+} from the cytoplasm to the lumen through the P-type ATPase Pmc1 and the Ca^{2+}/H^{+} antiporter Vcx1. Previously, we showed that Ca^{2+} uptake is blocked by verapamil when added at T=0, which looks like the effects of LPC-14 and LPC-18:0 and to a lesser extent LPC-18:1. On the other hand, LPC-

16 and LPA-18:1 have no effect on uptake; however, LPC-16 completely blocks Ca^{2+} efflux. This eliminates the possibility of causing lysis or transient pores to release Ca^{2+} as seen in lymphoma cells (12). When added late in the reaction we previously showed that verapamil caused a rapid release of Ca^{2+}, suggesting that Pmc1 activity continues throughout the reaction in part to balance the release of Ca^{2+}. Here, only LPC-18:1 appears to cause a rapid release at 250 μM while lower concentrations blocked release. Otherwise, only LPC-16 and LPA-18:1 were able to block Ca^{2+} efflux.

Ca^{2+} release from vacuoles under fusion conditions remains enigmatic as only one efflux channel has been identified and which has been shown not to participate in efflux during vacuole fusion (28, 29). During fission triggered by osmotic shock the TRPML1 homolog Yvc1 releases Ca^{2+} in a $PI(3,5)P_2$ dependent manner (38). In our studies we have shown that Yvc1 is not responsible for Ca^{2+} release. This is due in part to post-translational modification of Yvc1 during shock where the inactive form becomes glutathionylated by Gtt1 to become active (58, 59). This does not occur on isolated vacuoles under isotonic conditions. Thus, we conclude that the effects of lysolipids on Ca^{2+} transport are not linked to altering Yvc1 modification.

Regarding acidification, we believe this is the first documentation of lysolipids affecting V-ATPase function, suggesting that changes in curvature regulate its function. In contrast, mitochondrial F_1-F_O ATPase is the one to induce positive curvature through its multimerization (60, 61). Proton pumping can also be affected by changes in membrane fluidity. For instance, the plasma membrane H^+-ATPase Pma1 in *S. cerevisiae* is inhibited by decanoic acid which increases membrane fluidity (62). This is not due to changes in curvature as free fatty acids quickly equilibrate across the membrane bilayer. V-ATPase activity has also been linked to its interactions with cholesterol-rich microdomains in tumor cells (63). Depletion of cholesterol with methyl-β-cyclodextrin, and hence increasing fluidity reduced pumping activity and rates of cell migration. In our hands, increasing fluidity with dibucaine or deleting *ELO3* attenuates V-ATPase function (27).

While little is known about membrane curvature and V-ATPase function, we previously showed that it is interdependent with Ca^{2+} gradients (48). The addition of Ca^{2+} to acidification reactions show that V-ATPase function is inhibited in a dose dependent manner. This is dependent on the Ca^{2+}/H^+ exchanger Vcx1 as its deletion rendered vacuole acidification resistant to extraluminal Ca^{2+}. Conversely, Ca^{2+} transport required vacuole acidification. Both chloroquine and the V-ATPase inhibitor Bafilomycin block Ca^{2+} uptake and maintaining the Ca^{2+} gradient. This raises

the question as to whether LPLs affect acidification and Ca^{2+} transport in a similar interdependent way. Proteomic studies have shown that Vcx1 physically interacts with the V_O subunits Vma6 and Vph1, in addition to the V_1 subunits Vma1, Vma2, Vma4, Vma10 and Vma13 (64, 65). We found that LPC-14 blocks Ca^{2+} when added at T=0 min and not at T=10 min. This correlates with blocked acidification when LPC-14 is added at T=0 min and not T= 500 sec. Similar effects are seen with LPC-18:0 and LPC-18:1, albeit to different degrees. These outcomes are in keeping with the role of Vcx1 linking Ca^{2+} and H^+ transport, however, it is not universal for all LPCs tested. When looking at LPC-16, we saw that it does not affect Ca^{2+} uptake, yet it blocks acidification. A similar relationship occurs when LPC-16 is added later in the reactions. Another inconsistency is seen with LPA, which has no effect on Ca^{2+} or H^+ transport when added at T=0. When added late, LPA can inhibit Ca^{2+} release and yet it has no effect on vacuole acidification. This lack of an effect on acidification could be because Ca^{2+} did not accumulate outside the vacuole and instead was retained in the lumen.

Together these data show that Ca^{2+} and H^+ transport across the vacuole membrane is affected differently by LPLs depending on acyl chain length, but not monounsaturation. The size of lysolipid head group is also important through inducing more severe changes in curvature.

EXPERIMENTAL PROCEDURES

Reagents. Reagents were solubilized in PIPES-Sorbitol (PS) buffer (20 mM PIPES-KOH, pH 6.8, 200 mM sorbitol) with 125 mM KCl unless indicated otherwise. Anti-Sec17 IgG (44) and Pbi2 (66) were prepared as described previously. ATP was purchased from RPI (Mount Prospect, IL). Creatine phosphate was from Abcam (Waltham, MA). Acridine orange, Coenzyme A (CoA), Creatine kinase, and FCCP (Carbonyl cyanide-4-(trifluoromethoxy) phenylhydrazone) were purchased from Sigma (St. Louis, MO) and dissolved in PS buffer or DMSO. Cal-520 dextran conjugate MW, 10,000 (Cal-520) was from AAT Bioquest (Sunnyvale, CA) and dissolved in DMSO. 1-myristoyl-2-hydroxy-sn-glycerol-3-phosphocholine (Lysophosphatidylcholine, 14:0 LPC), and 1-stearoyl-2-hydroxy-sn-glycero-3-phosphocholine (18:0 LPC) were purchased from Cayman Chemical (Ann Arbor, MI) and dissolved in ethanol. 1-oleoyl-2-hydroxy-sn-glycero-3-phosphocholine (18:1-LPC) was from Avanti Polar Lipids (Birmingham, AL) was dissolved in ethanol. 1-oleoyl-2-hydroxy-sn-3-glycerophophate (18:1 lysophosphatidic acid, LPA) was purchased from Enzo Life Sciences (Farmingdale, NY) as was dissolved in PS buffer.

Vacuole isolation and in vitro content mixing

Yeast vacuoles were isolated from BJ3505 (*pep4Δ PHO8)* and DKY6281 (*PEP4 pho8Δ*) as described with modifications (33, 34, 67). Content mixing reactions (30 µL) contained 3 µg each of vacuoles from BJ3505 and DKY6281 backgrounds in fusion reaction buffer composed of PS buffer, 125 mM KCl, 5 mM $MgCl_2$, ATP regenerating system (ARS: 1 mM ATP, 0.1 mg/mL creatine kinase, 29 mM creatine phosphate), 10 µM CoA, and 280 nM recombinant Pbi2 (IB_2, Protease B inhibitor)(66). Reactions were incubated at 27°C and Pho8 activity was assayed in 250 mM Tris-Cl, pH 8.5, 0.4% Triton X-100, 10 mM $MgCl_2$, 1 mM *p*-nitrophenyl phosphate. Fusion was monitored as the absorbance at 400 nm from *p*-nitrophenolate production through phosphatase activity.

Vacuole acidification

Vacuole acidification by the V-ATPase was determined as described previously (48, 49, 68). Individual *in vitro* reactions (60 µl) contained 20 µg BJ3505 vacuoles, reaction buffer, ARS, 10 µM CoA, 283 nM Pbi2, and 15 µM AO. Reactions were set in a nonbinding black half-volume 96-well flat-bottom plate. Test reagents or PS buffer was added, and reactions were incubated at 27°C for 60 sec after which ATP regenerating system was added to each well. One well received additional PS buffer in place of ATP to serve as a negative control. AO fluorescence (ex 485 nm; em 520 nm) was measured in a fluorescence plate reader (POLARstar Omega, BMG Labtech) and readings were taken every 20 sec. After AO fluorescence plateaued (400-600 sec), each well received 30 µM FCCP (Carbonyl cyanide-4-(trifluoromethoxy) phenylhydrazone) to collapse the proton gradient and restore AO fluorescence. Each trace was normalized to the fluorescence intensities at the time of adding ATP and set to 1.

Calcium transport.

Ca^{2+} transport across the vacuole membrane was detected as described previously (29, 42, 43, 49). Ca^{2+} transport reactions (60 µl) contained 20 µg vacuoles isolated from BJ3505, reaction buffer, 10 µM CoA, 283 nM Pbi2, and 150 nM of the Ca^{2+} probe Cal520 dextran conjugate MW 10,000. Reactions were transferred to wells of a black, half-volume 96-well flat-bottom plate with nonbinding surface. Reactions were incubated at 27°C for 5 min after which ARS was added to each well. For a negative control one well received addition PS buffer in lieu of ATP. Reactions were analyzed using a fluorescence plate reader (ex 485 nm and em 520 nm). SNARE-dependent Ca^{2+} efflux was blocked with antibody against the SNARE co-chaperone Sec17. This served as

a negative control for SNARE function (28). Anti-Sec17 was prepared as described (44). Fluorescence readings were taken every 30 seconds for 120 min and normalized to the initial fluorescence value set to 1 for each reaction.

Statistical analysis

Results were expressed as the mean ± SEM. Experimental replicates (n) are defined as the number of separate experiments. Statistical analysis was performed by One-Way ANOVA for multiple comparisons using Prism 10 (GraphPad, San Diego, CA). Statistical significance is represented as follows: *$p<0.05$, ** $p<0.01$, *** $p<0.001$, **** $p<0.0001$. Tukey or Dunnett post hoc analysis was used for multiple comparisons and individual p-values.

Author Contribution

C.Z., Y.F. R.A.F., conceptualization; C.Z., Y.F. J.D.C, A.B., R.A, R.A.F., data curation; C.Z., Y.F. J.D.C, R.A.F., formal analysis; C.Z., R.A.F., writing original draft; C.Z., Y.F. J.D.C, A.B., R.A, R.A.F., writing-revision and editing; R.A.F., funding acquisition; R.A.F., supervision; R.A.F., project administration; R.A.F., resources.

Acknowledgements

This research was supported by grants from the National Science Foundation (MCB1818310 and MCB2216742 to RAF). JDC was partially supported by an NIGMS-NIH Chemistry-Biology Interface Training Grant (5T32-GM070421).

Conflict of interest

The authors declare that they have no conflict of interest.

References

1. Overduin, M., and Kervin, T. A. (2021) The phosphoinositide code is read by a plethora of protein domains. *Expert Rev. Proteomics*. **18**, 483–502
2. Lemmon, M. A. (2008) Membrane recognition by phospholipid-binding domains. *Nat. Rev. Mol. Cell Biol.* **9**, 99–111
3. Balla, T. (2013) Phosphoinositides: Tiny Lipids With Giant Impact on Cell Regulation. *Physiol. Rev.* **93**, 1019–1137

4. Andersen, O. S., and Koeppe, R. E. (2007) Bilayer thickness and membrane protein function: an energetic perspective. *Annu. Rev. Biophys. Biomol. Struct.* **36**, 107–130
5. Levental, I., and Lyman, E. (2023) Regulation of membrane protein structure and function by their paralipidomes. *Nat. Rev. Mol. Cell Biol.* **24**, 107–122
6. Harayama, T., and Riezman, H. (2018) Understanding the diversity of membrane lipid composition. *Nat. Rev. Mol. Cell Biol.* **19**, 281–296
7. Razinkov, V. I., Melikyan, G. B., Epand, R. M., Epand, R. F., and Cohen, F. S. (1998) Effects of spontaneous bilayer curvature on influenza virus-mediated fusion pores. *J. Gen. Physiol.* **112**, 409–422
8. Fuller, N., and Rand, R. P. (2001) The Influence of Lysolipids on the Spontaneous Curvature and Bending Elasticity of Phospholipid Membranes. *Biophys. J.* **81**, 243–254
9. Mohandas, N., Greenquist, A. C., and Shohet, S. B. (1978) Bilayer balance and regulation of red cell shape changes. *J. Supramol. Struct.* **9**, 453–458
10. Lundbaek, J. A., and Andersen, O. S. (1994) Lysophospholipids modulate channel function by altering the mechanical properties of lipid bilayers. *J. Gen. Physiol.* **104**, 645–673
11. Tokumura, A., Mostafa, M. H., Nelson, D. R., and Hanahan, D. J. (1985) Stimulation of (Ca2+ + Mg2+)-ATPase activity in human erythrocyte membranes by synthetic lysophosphatidic acids and lysophosphatidylcholines. Effects of chain length and degree of unsaturation of the fatty acid groups. *Biochim. Biophys. Acta*. **812**, 568–574
12. Wilson-Ashworth, H. A., Judd, A. M., Law, R. M., Freestone, B. D., Taylor, S., Mizukawa, M. K., Cromar, K. R., Sudweeks, S., and Bell, J. D. (2004) Formation of transient non-protein calcium pores by lysophospholipids in S49 Lymphoma cells. *J. Membr. Biol.* **200**, 25–33
13. Flemming, P. K., Dedman, A. M., Xu, S.-Z., Li, J., Zeng, F., Naylor, J., Benham, C. D., Bateson, A. N., Muraki, K., and Beech, D. J. (2006) Sensing of lysophospholipids by TRPC5 calcium channel. *J. Biol. Chem.* **281**, 4977–4982
14. Melikyan, G. B., Brener, S. A., Ok, D. C., and Cohen, F. S. (1997) Inner but not outer membrane leaflets control the transition from glycosylphosphatidylinositol-anchored influenza hemagglutinin-induced hemifusion to full fusion. *J. Cell Biol.* **136**, 995–1005
15. Shin, L., Wang, S., Lee, J.-S., Flack, A., Mao, G., and Jena, B. P. (2012) Lysophosphatidylcholine inhibits membrane-associated SNARE complex disassembly. *J. Cell. Mol. Med.* **16**, 1701–1708
16. Wu, H., Zheng, L., and Lentz, B. R. (1996) A slight asymmetry in the transbilayer distribution of lysophosphatidylcholine alters the surface properties and poly(ethylene glycol)-mediated fusion of dipalmitoylphosphatidylcholine large unilamellar vesicles. *Biochemistry*. **35**, 12602–12611
17. Chernomordik, L. V., Vogel, S. S., Sokoloff, A., Onaran, H. O., Leikina, E. A., and Zimmerberg, J. (1993) Lysolipids reversibly inhibit Ca(2+)-, GTP- and pH-dependent fusion of biological membranes. *FEBS Lett.* **318**, 71–76
18. Chernomordik, L. V., Leikina, E., Frolov, V., Bronk, P., and Zimmerberg, J. (1997) An early stage of membrane fusion mediated by the low pH conformation of influenza hemagglutinin depends upon membrane lipids. *J. Cell Biol.* **136**, 81–93
19. Melikyan, G. B., Markosyan, R. M., Hemmati, H., Delmedico, M. K., Lambert, D. M., and Cohen, F. S. (2000) Evidence that the transition of HIV-1 gp41 into a six-helix bundle, not the bundle configuration, induces membrane fusion. *J. Cell Biol.* **151**, 413–423

20. Kato, M., and Wickner, W. (2001) Ergosterol is required for the Sec18/ATP-dependent priming step of homotypic vacuole fusion. *EMBO J.* **20**, 4035–4040
21. Mayer, A., Scheglmann, D., Dove, S., Glatz, A., Wickner, W., and Haas, A. (2000) Phosphatidylinositol 4,5-bisphosphate regulates two steps of homotypic vacuole fusion. *Mol. Biol. Cell*. **11**, 807–817
22. Miner, G. E., Starr, M. L., Hurst, L. R., Sparks, R. P., Padolina, M., and Fratti, R. A. (2016) The Central Polybasic Region of the Soluble SNARE (Soluble N-Ethylmaleimide-sensitive Factor Attachment Protein Receptor) Vam7 Affects Binding to Phosphatidylinositol 3-Phosphate by the PX (Phox Homology) Domain. *J. Biol. Chem.* **291**, 17651–17663
23. Starr, M. L., Sparks, R. P., Arango, A. S., Hurst, L. R., Zhao, Z., Lihan, M., Jenkins, J. L., Tajkhorshid, E., and Fratti, R. A. (2019) Phosphatidic acid induces conformational changes in Sec18 protomers that prevent SNARE priming. *J. Biol. Chem.* **294**, 3100–3116
24. Stroupe, C., Collins, K. M., Fratti, R. A., and Wickner, W. (2006) Purification of active HOPS complex reveals its affinities for phosphoinositides and the SNARE Vam7p. *EMBO J.* **25**, 1579–1589
25. Lawrence, G., Brown, C. C., Flood, B. A., Karunakaran, S., Cabrera, M., Nordmann, M., Ungermann, C., and Fratti, R. A. (2014) Dynamic association of the PI3P-interacting Mon1-Ccz1 GEF with vacuoles is controlled through its phosphorylation by the type 1 casein kinase Yck3. *Mol. Biol. Cell*. **25**, 1608–1619
26. Cabrera, M., Nordmann, M., Perz, A., Schmedt, D., Gerondopoulos, A., Barr, F., Piehler, J., Engelbrecht-Vandré, S., and Ungermann, C. (2014) The Mon1-Ccz1 GEF activates the Rab7 GTPase Ypt7 via a longin-fold-Rab interface and association with PI3P-positive membranes. *J. Cell Sci.* **127**, 1043–1051
27. Zhang, C., Calderin, J. D., Hurst, L. R., Gokbayrak, Z. D., Hrabak, M. R., Balutowski, A., Rivera-Kohr, D. A., Kazmirchuk, T. D. D., Brett, C. L., and Fratti, R. A. (2024) Sphingolipids containing very long-chain fatty acids regulate Ypt7 function during the tethering stage of vacuole fusion. *J. Biol. Chem.* 10.1016/j.jbc.2024.107808
28. Merz, A. J., and Wickner, W. T. (2004) Trans-SNARE interactions elicit Ca2+ efflux from the yeast vacuole lumen. *J. Cell Biol.* **164**, 195–206
29. Miner, G. E., Sullivan, K. D., Zhang, C., Rivera-Kohr, D., Guo, A., Hurst, L. R., Ellis, E. C., Starr, M. L., Jones, B. C., and Fratti, R. A. (2020) Phosphatidylinositol 3,5-bisphosphate regulates Ca2+ transport during yeast vacuolar fusion through the Ca2+ ATPase Pmc1. *Traffic Cph. Den.* **21**, 503–517
30. Miner, G. E., Sullivan, K. D., Guo, A., Jones, B. C., Hurst, L. R., Ellis, E. C., Starr, M. L., and Fratti, R. A. (2019) Phosphatidylinositol 3,5-bisphosphate regulates the transition between trans-SNARE complex formation and vacuole membrane fusion. *Mol. Biol. Cell*. **30**, 201–208
31. Peters, C., Bayer, M. J., Bühler, S., Andersen, J. S., Mann, M., and Mayer, A. (2001) Trans-complex formation by proteolipid channels in the terminal phase of membrane fusion. *Nature*. **409**, 581–588
32. Reese, C., and Mayer, A. (2005) Transition from hemifusion to pore opening is rate limiting for vacuole membrane fusion. *J. Cell Biol.* **171**, 981–990

33. Jones, E. W., Zubenko, G. S., and Parker, R. R. (1982) PEP4 gene function is required for expression of several vacuolar hydrolases in Saccharomyces cerevisiae. *Genetics*. **102**, 665–677
34. Klionsky, D. J., and Emr, S. D. (1989) Membrane protein sorting: biosynthesis, transport and processing of yeast vacuolar alkaline phosphatase. *EMBO J.* **8**, 2241–2250
35. Dunn, T., Gable, K., and Beeler, T. (1994) Regulation of cellular Ca2+ by yeast vacuoles. *J. Biol. Chem.* **269**, 7273–7278
36. Cunningham, K. W., and Fink, G. R. (1994) Calcineurin-dependent growth control in Saccharomyces cerevisiae mutants lacking PMC1, a homolog of plasma membrane Ca2+ ATPases. *J. Cell Biol.* **124**, 351–363
37. Cunningham, K. W., and Fink, G. R. (1996) Calcineurin inhibits VCX1-dependent H+/Ca2+ exchange and induces Ca2+ ATPases in Saccharomyces cerevisiae. *Mol. Cell. Biol.* **16**, 2226–2237
38. Denis, V., and Cyert, M. S. (2002) Internal Ca(2+) release in yeast is triggered by hypertonic shock and mediated by a TRP channel homologue. *J. Cell Biol.* **156**, 29–34
39. Bonangelino, C. J., Nau, J. J., Duex, J. E., Brinkman, M., Wurmser, A. E., Gary, J. D., Emr, S. D., and Weisman, L. S. (2002) Osmotic stress-induced increase of phosphatidylinositol 3,5-bisphosphate requires Vac14p, an activator of the lipid kinase Fab1p. *J. Cell Biol.* **156**, 1015–1028
40. Dong, X., Shen, D., Wang, X., Dawson, T., Li, X., Zhang, Q., Cheng, X., Zhang, Y., Weisman, L. S., Delling, M., and Xu, H. (2010) PI(3,5)P(2) controls membrane trafficking by direct activation of mucolipin Ca(2+) release channels in the endolysosome. *Nat. Commun.* **1**, 38
41. Su, Z., Anishkin, A., Kung, C., and Saimi, Y. (2011) The core domain as the force sensor of the yeast mechanosensitive TRP channel. *J. Gen. Physiol.* **138**, 627–640
42. Sasser, T. L., Padolina, M., and Fratti, R. A. (2012) The yeast vacuolar ABC transporter Ybt1p regulates membrane fusion through Ca2+ transport modulation. *Biochem. J.* **448**, 365–372
43. Miner, G. E., and Fratti, R. (2019) Real-Time Fluorescence Detection of Calcium Efflux During Vacuolar Membrane Fusion. *Methods Mol. Biol. Clifton NJ*. **1860**, 323–331
44. Mayer, A., Wickner, W., and Haas, A. (1996) Sec18p (NSF)-driven release of Sec17p (alpha-SNAP) can precede docking and fusion of yeast vacuoles. *Cell*. **85**, 83–94
45. Kooijman, E. E., Chupin, V., de Kruijff, B., and Burger, K. N. J. (2003) Modulation of membrane curvature by phosphatidic acid and lysophosphatidic acid. *Traffic Cph. Den.* **4**, 162–174
46. Banerjee, S., Clapp, K., Tarsio, M., and Kane, P. M. (2019) Interaction of the late endo-lysosomal lipid PI(3,5)P2 with the Vph1 isoform of yeast V-ATPase increases its activity and cellular stress tolerance. *J. Biol. Chem.* **294**, 9161–9171
47. Li, S. C., Diakov, T. T., Xu, T., Tarsio, M., Zhu, W., Couoh-Cardel, S., Weisman, L. S., and Kane, P. M. (2014) The signaling lipid PI(3,5)P_2 stabilizes V_1-V(o) sector interactions and activates the V-ATPase. *Mol. Biol. Cell*. **25**, 1251–1262
48. Zhang, C., Feng, Y., Balutowski, A., Miner, G. E., Rivera-Kohr, D. A., Hrabak, M. R., Sullivan, K. D., Guo, A., Calderin, J. D., and Fratti, R. A. (2022) The interdependent transport of yeast vacuole Ca2+ and H+ and the role of Phosphatidylinositol 3,5-bisphosphate. *J. Biol. Chem.* 10.1016/j.jbc.2022.102672

49. Zhang, C., Balutowski, A., Feng, Y., Calderin, J. D., and Fratti, R. A. (2022) High throughput analysis of vacuolar acidification. *Anal. Biochem.* **658**, 114927
50. Moriyama, Y., Takano, T., and Ohkuma, S. (1982) Acridine orange as a fluorescent probe for lysosomal proton pump. *J. Biochem. (Tokyo)*. **92**, 1333–1336
51. Thomé, M. P., Filippi-Chiela, E. C., Villodre, E. S., Migliavaca, C. B., Onzi, G. R., Felipe, K. B., and Lenz, G. (2016) Ratiometric analysis of Acridine Orange staining in the study of acidic organelles and autophagy. *J. Cell Sci.* **129**, 4622–4632
52. Pierzyńska-Mach, A., Janowski, P. A., and Dobrucki, J. W. (2014) Evaluation of acridine orange, LysoTracker Red, and quinacrine as fluorescent probes for long-term tracking of acidic vesicles. *Cytom. Part J. Int. Soc. Anal. Cytol.* **85**, 729–737
53. Kooijman, E. E., Chupin, V., Fuller, N. L., Kozlov, M. M., de Kruijff, B., Burger, K. N. J., and Rand, P. R. (2005) Spontaneous curvature of phosphatidic acid and lysophosphatidic acid. *Biochemistry*. **44**, 2097–2102
54. Golfman, L. S., Haughey, N. J., Wong, J. T., Jiang, J. Y., Lee, D., Geiger, J. D., and Choy, P. C. (1999) Lysophosphatidylcholine induces arachidonic acid release and calcium overload in cardiac myoblastic H9c2 cells. *J. Lipid Res.* **40**, 1818–1826
55. Wang, P., Wang, Q., Yang, L., Qin, Q.-L., and Wu, Y.-J. (2015) Characterization of lysophosphatidylcholine-induced changes of intracellular calcium in Drosophila S2 cells. *Life Sci.* **131**, 57–62
56. Monet, M., Gkika, D., Lehen'kyi, V., Pourtier, A., Vanden Abeele, F., Bidaux, G., Juvin, V., Rassendren, F., Humez, S., and Prevarsakaya, N. (2009) Lysophospholipids stimulate prostate cancer cell migration via TRPV2 channel activation. *Biochim. Biophys. Acta*. **1793**, 528–539
57. Ohata, H., Tanaka, K., Aizawa, H., Ao, Y., Iijima, T., and Momose, K. (1997) Lysophosphatidic acid sensitises Ca2+ influx through mechanosensitive ion channels in cultured lens epithelial cells. *Cell. Signal.* **9**, 609–616
58. Chandel, A., Das, K. K., and Bachhawat, A. K. (2016) Glutathione depletion activates the yeast vacuolar transient receptor potential channel, Yvc1p, by reversible glutathionylation of specific cysteines. *Mol. Biol. Cell*. **27**, 3913–3925
59. Hamamoto, S., Mori, Y., Yabe, I., and Uozumi, N. (2018) In vitro and in vivo characterization of modulation of the vacuolar cation channel TRPY1 from Saccharomyces cerevisiae. *FEBS J.* **285**, 1146–1161
60. Jiko, C., Davies, K. M., Shinzawa-Itoh, K., Tani, K., Maeda, S., Mills, D. J., Tsukihara, T., Fujiyoshi, Y., Kühlbrandt, W., and Gerle, C. (2015) Bovine F1Fo ATP synthase monomers bend the lipid bilayer in 2D membrane crystals. *eLife*. **4**, e06119
61. Blum, T. B., Hahn, A., Meier, T., Davies, K. M., and Kühlbrandt, W. (2019) Dimers of mitochondrial ATP synthase induce membrane curvature and self-assemble into rows. *Proc. Natl. Acad. Sci. U. S. A.* **116**, 4250–4255
62. Alexandre, H., Mathieu, B., and Charpentier, C. (1996) Alteration in membrane fluidity and lipid composition, and modulation of H(+)-ATPase activity in Saccharomyces cerevisiae caused by decanoic acid. *Microbiol. Read. Engl.* **142 (Pt 3)**, 469–475
63. Costa, G. A., de Souza, S. B., da Silva Teixeira, L. R., Okorokov, L. A., Arnholdt, A. C. V., Okorokova-Façanha, A. L., and Façanha, A. R. (2018) Tumor cell cholesterol depletion and

V-ATPase inhibition as an inhibitory mechanism to prevent cell migration and invasiveness in melanoma. *Biochim. Biophys. Acta Gen. Subj.* **1862**, 684–691
64. Khan, M. M., Lee, S., Couoh-Cardel, S., Oot, R. A., Kim, H., Wilkens, S., and Roh, S.-H. (2022) Oxidative stress protein Oxr1 promotes V-ATPase holoenzyme disassembly in catalytic activity-independent manner. *EMBO J.* **41**, e109360
65. Michaelis, A. C., Brunner, A.-D., Zwiebel, M., Meier, F., Strauss, M. T., Bludau, I., and Mann, M. (2023) The social and structural architecture of the yeast protein interactome. *Nature*. **624**, 192–200
66. Slusarewicz, P., Xu, Z., Seefeld, K., Haas, A., and Wickner, W. T. (1997) I2B is a small cytosolic protein that participates in vacuole fusion. *Proc. Natl. Acad. Sci. U. S. A.* **94**, 5582–5587
67. Haas, A., Conradt, B., and Wickner, W. (1994) G-protein ligands inhibit in vitro reactions of vacuole inheritance. *J. Cell Biol.* **126**, 87–97
68. Müller, O., Neumann, H., Bayer, M. J., and Mayer, A. (2003) Role of the Vtc proteins in V-ATPase stability and membrane trafficking. *J. Cell Sci.* **116**, 1107–1115

Notes

Current Addresses

Yilin Feng – Interdisciplinary Biological Sciences Graduate Program, Northwestern University, Evanston IL, 60208

Adam Balutowski – Department of Biochemistry, Washington University, St. Louis MO 63110

Abbreviations used

AO, acridine orange; ARS, ATP regeneration system; DAG, diacylglycerol; FCCP, Carbonyl cyanide-4-(trifluoromethoxy) phenylhydrazone; LPA, lysophosphatidic acid; LPC, lysophosphatidylcholine; LPE lysophosphatidylethanolamine; LPI, lysophosphatidylinositol; LPS, lysophosphatidylserine; NEM, n-ethylmaleimide; NSF, NEM sensitive factor; PA, phosphatidic acid; PC, phosphatidylcholine; PI, phosphatidylinositol; PLC, phospholipase C; SNARE, soluble NSF attachment protein receptor; TRP, transient receptor potential; YPD, yeast extract, peptone, dextrose.

Figures and Legends.

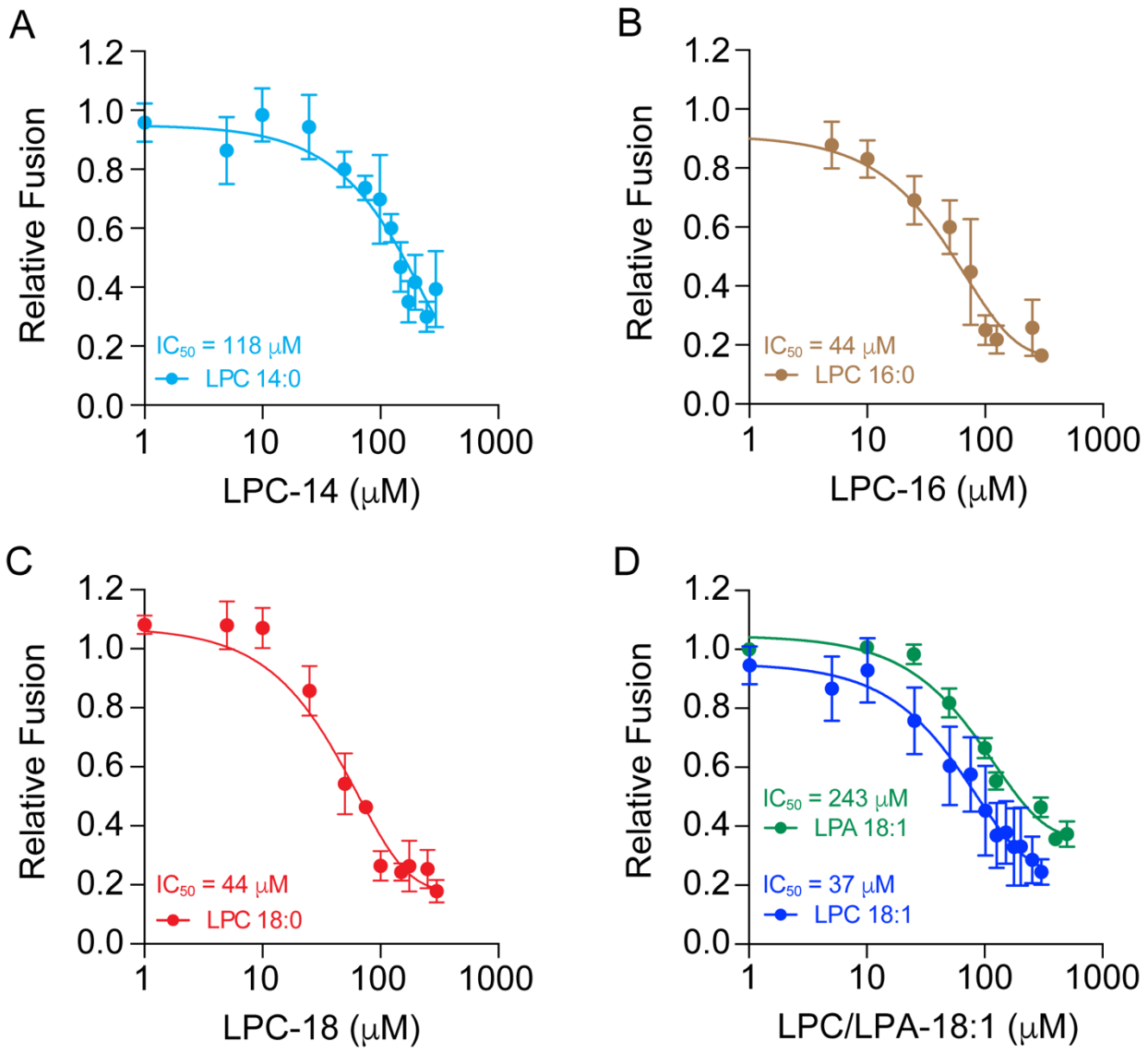

Figure 1. Inhibition of vacuole fusion by lysolipids. Vacuole fusion reactions were treated with dosage curves of lysolipids for 90 min at 27°C. Vacuole fusion reactions contained buffer or myristyl LPC-14 **(A)**, palmitoyl LPC-16 **(B),** stearoyl LPC-18:0 **(C)**, or oleoyl LPC-18:1 and LPA-18:1 **(D)**. Fusion was determined by measuring Pho8 activity and conversion of PNPP to PNP at 400 nm. Fusion values were normalized to the untreated control that is set to 1. Error bars represent SEM. N≥3.

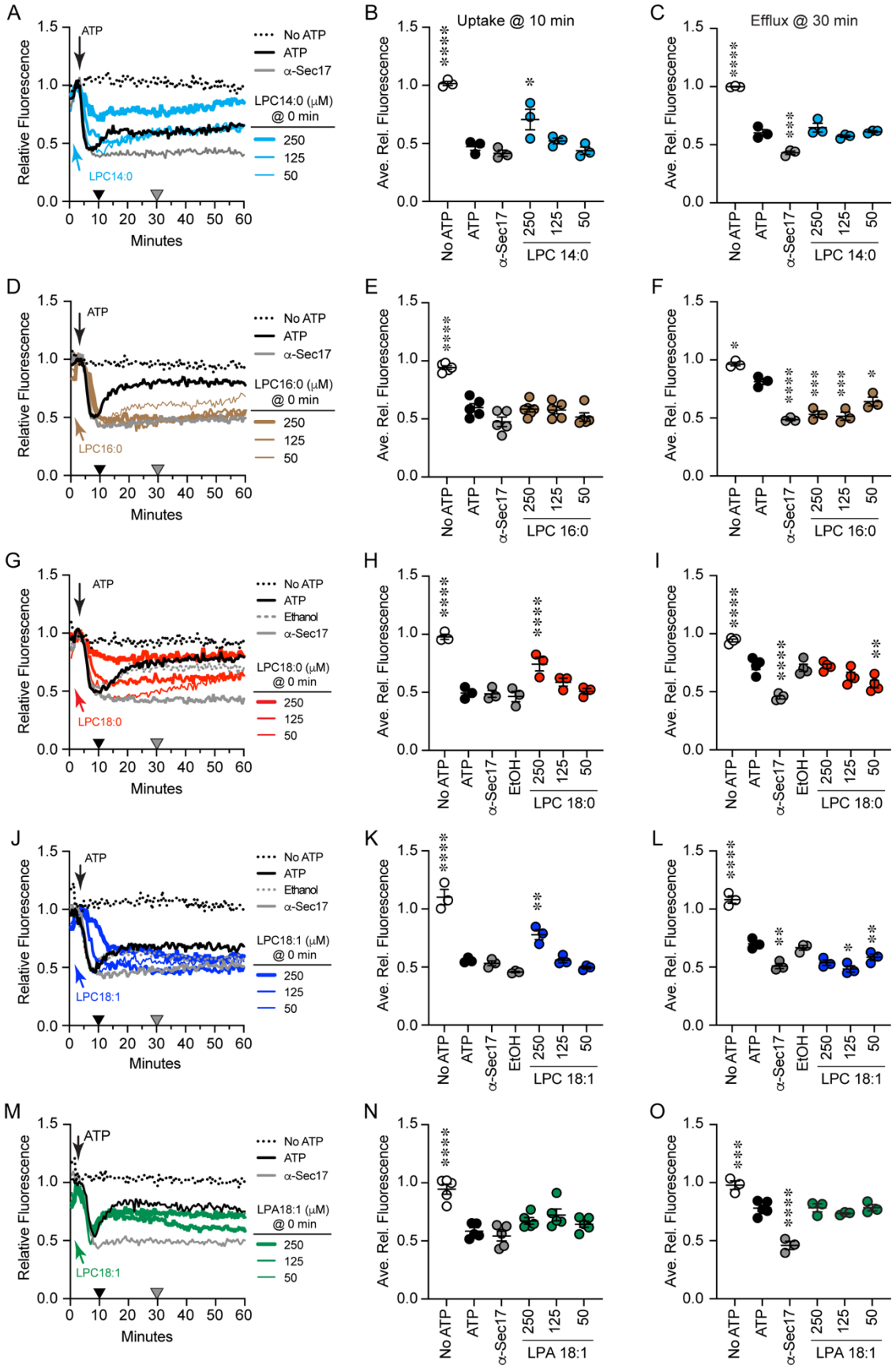
A
B
Uptake @ 10 min
C
Efflux @ 30 min
D
E
F
G
H
I
J
K
L
M
N
O
Relative Fluorescence
Minutes
ATP
No ATP
α-Sec17
Ethanol
LPC14:0 (μM) @ 0 min
LPC16:0 (μM) @ 0 min
LPC18:0 (μM) @ 0 min
LPC18:1 (μM) @ 0 min
LPA18:1 (μM) @ 0 min
250
125
50
LPC14:0
LPC16:0
LPC18:0
LPC18:1
Ave. Rel. Fluorescence
EtOH
LPC 14:0
LPC 16:0
LPC 18:0
LPC 18:1
LPA 18:1

Figure 2. Effect of lysolipids on Ca2+ uptake.

Vacuoles were isolated from BJ3505 and 2X fusion reactions (60 µL) were treated with 140 µg/mL α-Sec17 IgG, LPC variants or reaction buffer at T=0 min in the absence of ATP and in the presence of Cal520. Reactions contained LPC-14:0 **(A)**, LPC-16:0 **(D)**, LPC-18:0 **(G)**, LPC-18:1 **(J)**, or LPA-18:1 **(M)**. After 5 min of incubation ATP or buffer was added to each reaction. Cal520 fluorescence was monitored every 30 sec for 60 min. Fluorescence values were normalized to the untreated control at T=5 when ATP was added and set at 1. **(B, E, H, K, N)** Ca^{2+} uptake efficiency was quantified after 10 min of incubation (Black triangles). **(C, F, I, L, O)** SNARE-dependent Ca^{2+} efflux efficiency was quantified after 30 min incubation (Gray triangles). Error bars represent SEM ($n \geq 3$). Significance was measured using one way ANOVA for multiple comparisons. Tukey's post hoc test was used for individual p values. ***p*<0.01, ****p*<0.001, *****p*<0.0001.

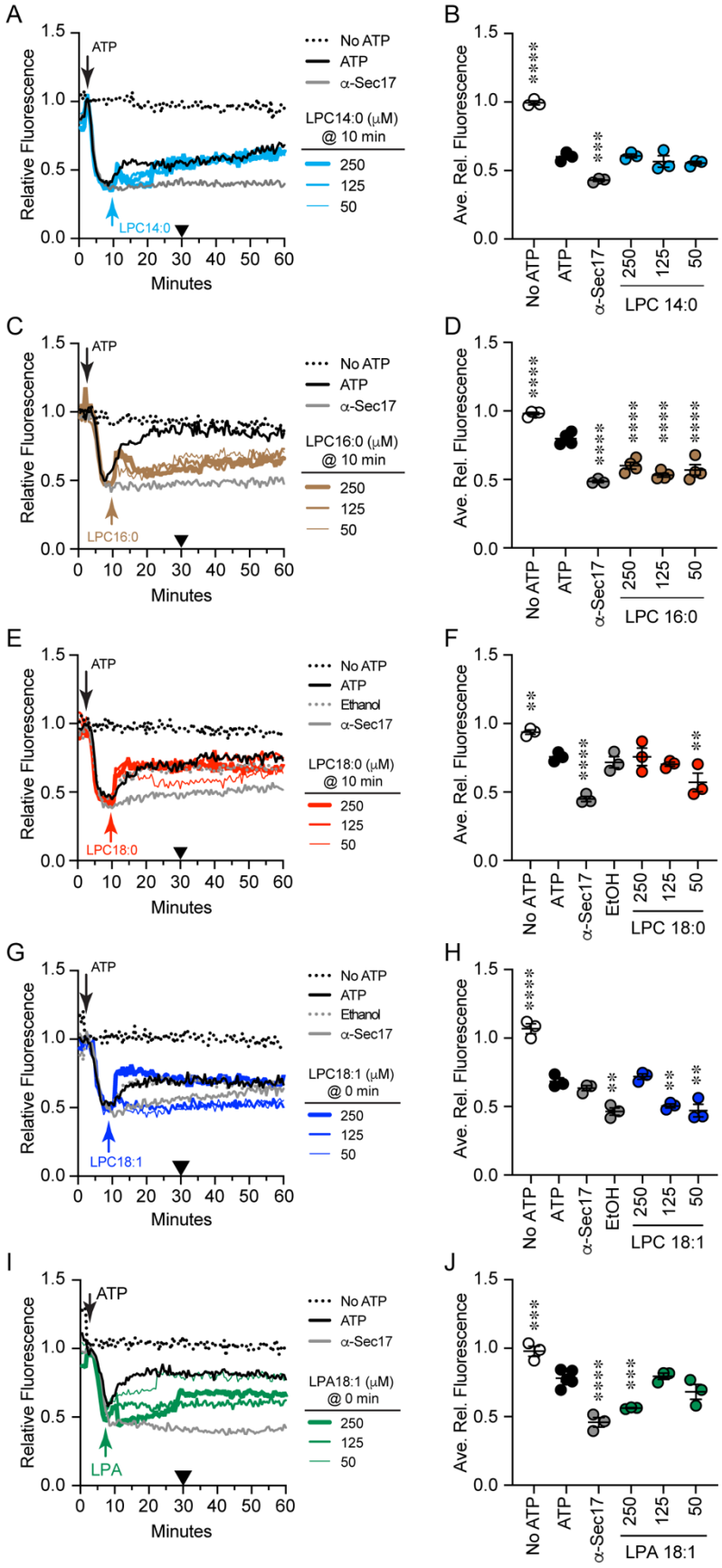
A
B
C
D
E
F
G
H
I
J
Relative Fluorescence
Minutes
ATP
LPC14:0
LPC16:0
LPC18:0
LPC18:1
LPA
No ATP
ATP
Ethanol
α-Sec17
LPC14:0 (μM) @ 10 min
LPC16:0 (μM) @ 10 min
LPC18:0 (μM) @ 10 min
LPC18:1 (μM) @ 0 min
LPA18:1 (μM) @ 0 min
250
125
50
Ave. Rel. Fluorescence
EtOH
LPC 14:0
LPC 16:0
LPC 18:0
LPC 18:1
LPA 18:1

Figure 3. Effect of lysolipids on Ca2+ uptake.

Vacuoles from BJ3505 were incubated as 2X fusion reactions (60 µL) and treated with 140 µg/mL α-Sec17 IgG at T=0 in the presence of Cal520. After 5 min of incubation ATP or buffer was added to each reaction. LPC variants were added after 10 min. Reactions contained LPC-14:0 **(A)**, LPC-16:0 **(C)**, LPC-18:0 **(E)**, LPC-18:1 **(G)**, or LPA-18:1 **(I)**. Cal520 fluorescence was monitored every 30 sec for 60 min. Fluorescence values were normalized to the untreated control at T=5 min when ATP was added and at 1. **(B, D, F, H, J)** SNARE-dependent Ca^{2+} efflux efficiency was quantified after 30 min incubation (Black triangles). Error bars represent SEM ($n \geq 3$). Significance was measured using one way ANOVA for multiple comparisons. Tukey's post hoc test was used for individual p values. *p<0.05, **p<0.01, ***p<0.001, ****p<0.0001.

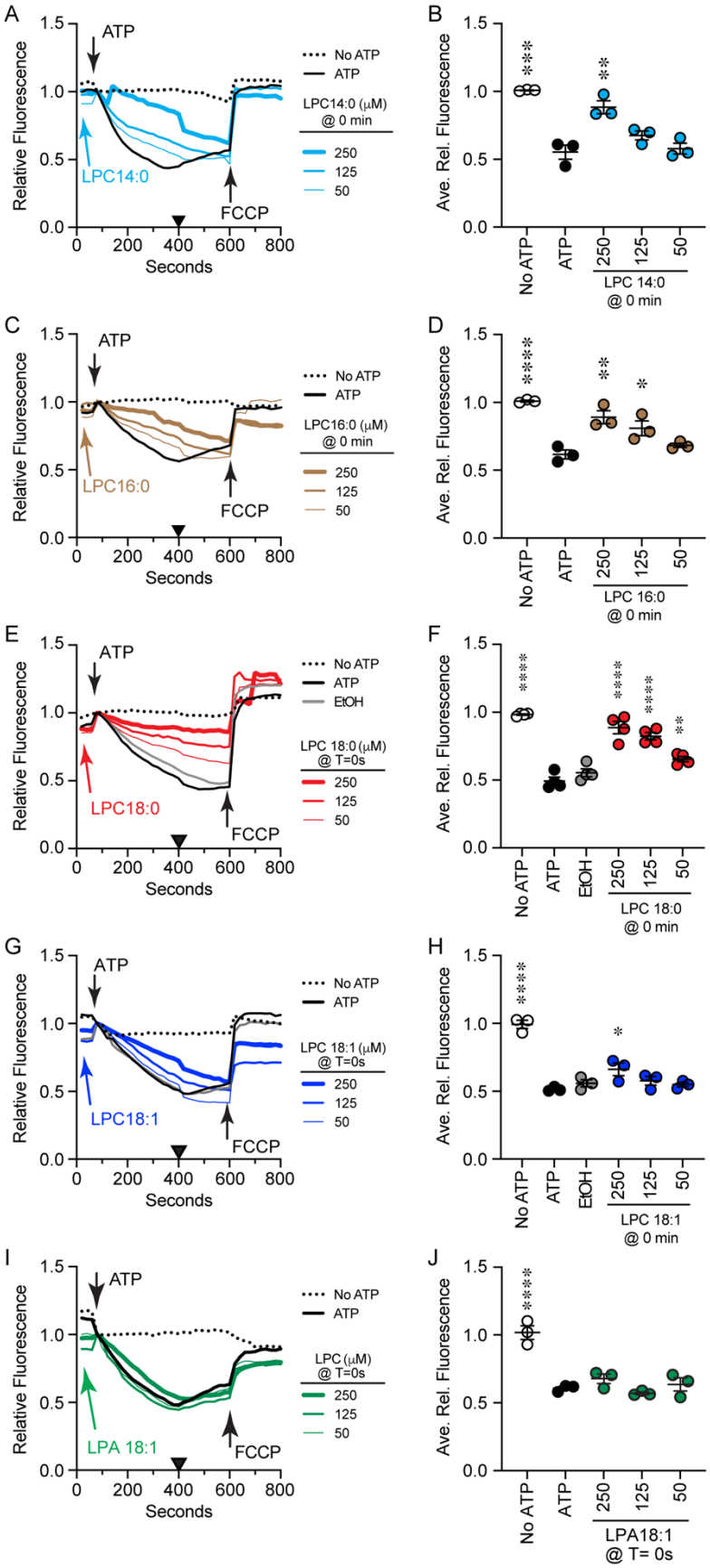
A
ATP
Relative Fluorescence
Seconds
No ATP
ATP
LPC14:0 (μM)
@ 0 min
250
125
50
LPC14:0
FCCP
B
Ave. Rel. Fluorescence
No ATP
ATP
LPC 14:0
@ 0 min
C
LPC16:0 (μM)
LPC16:0
D
LPC 16:0
E
EtOH
LPC 18:0 (μM)
@ T=0s
LPC18:0
F
LPC 18:0
G
LPC 18:1 (μM)
LPC18:1
H
LPC 18:1
I
LPC (μM)
LPA 18:1
J
LPA18:1
@ T= 0s

Figure 4. Effect of lysolipids on initial vacuole acidification.

BJ3505 vacuoles fusion reactions (2X) were incubated with LPC variants or reaction buffer at T=0 min in the absence of ATP and in the presence of AO. After 60 s of incubation received ATP or additional buffer and further incubated for a total of 800 s. After 600 s each reaction received FCCP to equilibrate the proton gradient. AO fluorescence was normalized to the fluoresced at the time of adding ATP set to 1. Separate experiments were treated with LPC-14:0 **(A)**, LPC-16:0 **(C)**, LPC-18:0 **(E)**, LPC-18:1 **(G)**, or LPA-18:1 **(I). (B, D, F, H, J)** Vacuole acidification efficiency was quantified after 400 s (Black triangles). Error bars represent SEM ($n \geq 3$). Significance was measured using one way ANOVA for multiple comparisons. Tukey's post hoc test was used for individual p values. *$p<0.05$, **$p<0.01$, ***$p<0.001$, ****$p<0.0001$.

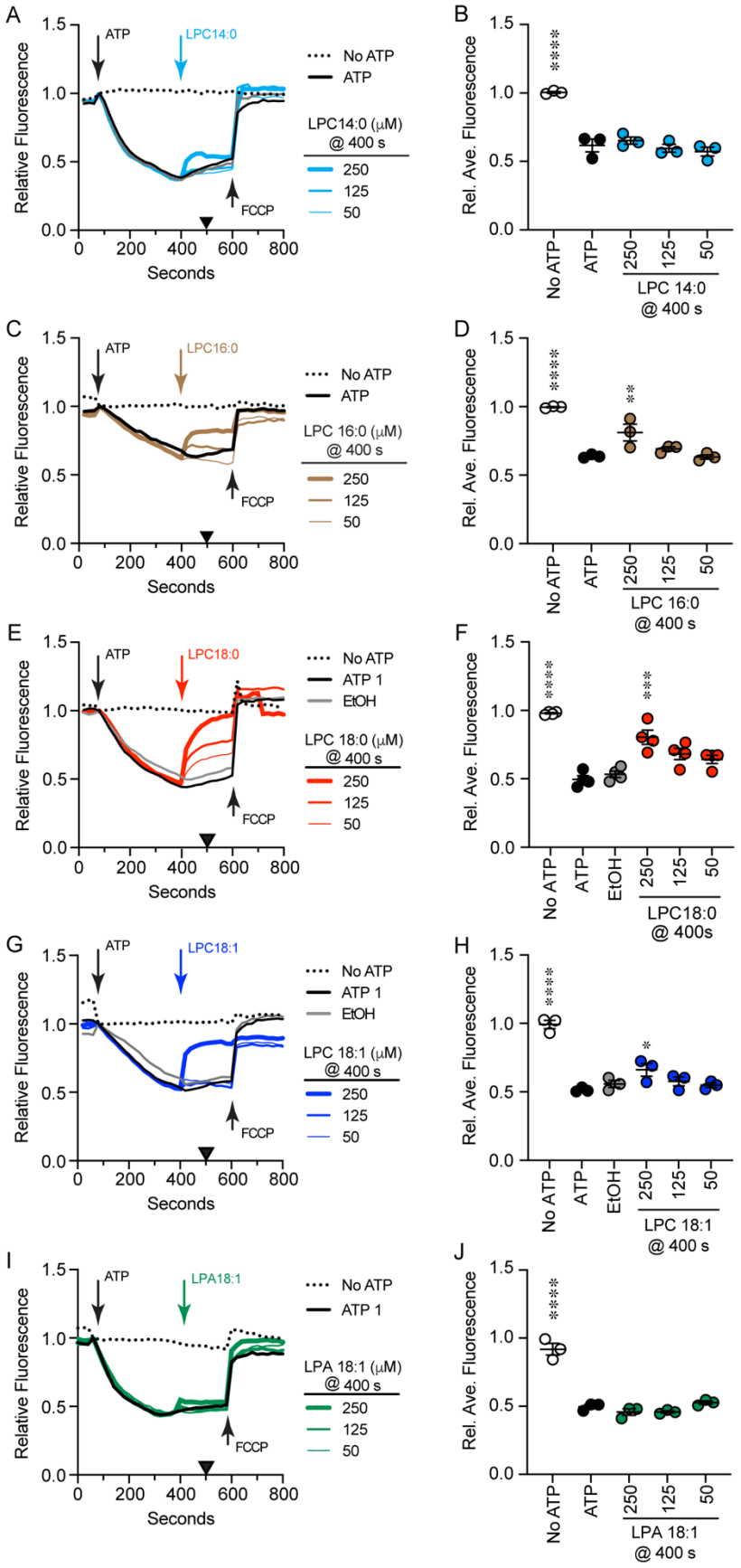
A
ATP
LPC14:0
No ATP
ATP
LPC14:0 (μM) @ 400 s
250
125
50
FCCP
Relative Fluorescence
Seconds
B
Rel. Ave. Fluorescence
No ATP
ATP
250
125
50
LPC 14:0 @ 400 s
C
ATP
LPC16:0
No ATP
ATP
LPC 16:0 (μM) @ 400 s
250
125
50
FCCP
Relative Fluorescence
Seconds
D
Rel. Ave. Fluorescence
No ATP
ATP
250
125
50
LPC 16:0 @ 400 s
E
ATP
LPC18:0
No ATP
ATP 1
EtOH
LPC 18:0 (μM) @ 400 s
250
125
50
FCCP
Relative Fluorescence
Seconds
F
Rel. Ave. Fluorescence
No ATP
ATP
EtOH
250
125
50
LPC18:0 @ 400s
G
ATP
LPC18:1
No ATP
ATP 1
EtOH
LPC 18:1 (μM) @ 400 s
250
125
50
FCCP
Relative Fluorescence
Seconds
H
Rel. Ave. Fluorescence
No ATP
ATP
EtOH
250
125
50
LPC 18:1 @ 400 s
I
ATP
LPA18:1
No ATP
ATP 1
LPA 18:1 (μM) @ 400 s
250
125
50
FCCP
Relative Fluorescence
Seconds
J
Rel. Ave. Fluorescence
No ATP
ATP
250
125
50
LPA 18:1 @ 400 s

Figure 5. Effect of lysolipids on maintaining vacuole acidification.

Vacuoles from BJ3505 were incubated as 2X fusion reactions (60 µL) and incubated with reaction buffer and AO at T=0 min. After 60 s of reactions received ATP or additional reaction buffer. LPC variants were added at 400 s. After 600 s each reaction received FCCP to equilibrate the proton gradient and further incubated for a total of 800 s. AO fluorescence was normalized to the fluoresced at the time of adding ATP set to 1. Separate experiments were treated with LPC-14:0 **(A)**, LPC-16:0 **(C)**, LPC-18:0 **(E)**, LPC-18:1 **(G)**, or LPA-18:1 **(I). (B, D, F, H, J)** Vacuole acidification efficiency was quantified after 400 s (Black triangles). Error bars represent SEM ($n \geq 3$). Significance was measured using one way ANOVA for multiple comparisons. Tukey's post hoc test was used for individual p values. ***$p<0.001$, ****$p<0.0001$.